Anal. Bioanal. Electrochem., Vol. 10, No. 10, 2018, 1355-1367

Analytical & Bioanalytical Electrochemistry

2018 by CEE
www.abechem.com

Full Paper

Cathodic Electrochemical Synthesis of Cerium Doped Iron Oxide and Investigation of its Charge Storage and Magnetic Properties

Mohammad Reza Ganjali [1,2,*] and Morteza Rezapour[3]

[1]*Center of Excellence in Electrochemistry, School of Chemistry, University of Tehran, Tehran, Iran*

[2]*Biosensor Research Center, Endocrinology & Metabolism Molecular-Cellular Sciences Institute, Tehran University of Medical Sciences, Tehran, Iran*

[3]*IP Department, Research Institute of the Petroleum Industry (RIPI), P.O. Box 14665-137, Tehran, Iran*

*Corresponding Author, E-Mail: ganjali@khayam.ut.ac.ir

Received: 18 May 2018 / Received in revised form: 31 August 2018 / Accepted: 2 September 2018 / Published online: 31 October 2018

Abstract- In this paper, cerium doped iron oxide (Ce-IO) is cathodically electro-synthesized from electrolyte containing iron(III) nitrate, iron(II) chloride and cerium chloride by applying direct current of 10 mA cm^{-2} for 30 min. The analysis data obtained from X-ray diffraction (XRD), field emission electron microscopy (FE-SEM) and energy-dispersive X-ray (EDX) showed that the synthesized Ce-IO sample has composition of cerium cations doped magnetite crystal structure and average particle size of 20 nm. This developed electrochemical procedure can be proposed as a one-pot electrosynthesis platform for fabrication of nanoparticles of cerium doped iron oxide. Furthermore, the prepared Ce-IO was used as supercapacitor electrode material and its charge storage ability was specified through cyclic voltammetry (CV) and galvanostat charge-discharge (GCD) tests. The obtained charge storage data indicated that Ce-IO sample provide SCs as high as 168 and 125 F g^{-1} at the discharge loads of 1 and 3 A g^{-1}, respectively, and capacity retentions of 90.4% and 81.5% after 1000 GCD cycling. These results proved the suitability of the electro-synthesized sample for use in supercapacitors. Also, the VSM data confirmed better superparamagnetic properties of Ce-IO sample (Mr=0.14 emu g^{-1} and H_{Ci}=2.44 G) as

compared with undoped iron oxide sample (Mr=0.95 emu g^{-1} and H_{Ci}=14.6 G) resulting from their lower *Mr* and *Hci* values.

Keywords- Iron oxide, Nanoparticles, Cerium doping, Electrosynthesis, Supercapacitors

1. INTRODUCTION

There are two electrochemical capacitors (ECs) models including electric double layer capacitors (EDLCs) and pseudocapacitors (PCs). EDLCs electrostatically store charges on their high surface interface of electrodes, and exhibit rapid charge storage with limited specific capacitances [1]. PCs mainly store charges from reversible Faradic reactions and generally composed of transition metal oxides/hydroxides such as tin oxide [2], cobalt oxides [3-5], cerium oxide [6], nickel oxide [7-9], titanium oxide [10], manganese oxides [11-17], cobalt hydroxides [18-28], nickel hydroxides [29-33] and iron oxides [34-40]. This type of SCs could deliver high specific capacitances, but present low cycle life. Among metal oxides, magnetite (Fe_3O_4) is the interested candidates as a result of its environmental friendliness, natural abundance, low cost and variable oxidation states [41]. Magnetite has low electrical conductivity, which referred as major obstacle for use in ECs [42,43]. For refine this issue, several works have been reported which are mixing with CNTs and GO [44-47], doping with metal cations [48], and preparing new nanostructures [49-56]. These researches have shown that performance of iron oxide material is improved as a result of enhancing the conductivity and faradic reactions.

In this paper, we report an electrochemical synthesis route for the preparing cerium ion doped iron oxide (Ce-IO) through CD procedure. This synthesis is based on the well-known cathodic deposition (CD). In this synthesis, nanostructured metal oxides/hydroxide could be easily prepared through OH^- generation on the cathode [57]. It should be noted that fine NPs of metal oxides and hydroxides have been synthesized through one-pot CD synthesis [10,11,21,31,58,59]. However, this method has been rarely used for the preparation of iron oxides (IOs). It is worth noting that one-pot electrosynthesis of bare- and surface coated IOs has been reported through CD method [60-63]. Here, we applied this deposition route for the fabricating cerium doped IO-NPs. The prepared Ce-IO sample was characterized by XRD, IR, FE-SEM, VSM, cyclic voltammetry (CV) and galvanostat charge-discharge (GCD) techniques. The results of these analyses showed the suitable magnetic and charge storage ability of the prepared cerium doped IO nanoparticles.

2. EXPERIMENTAL PROCEDURE

2.1. Materials

Ferrous chloride tetrahydrate ($FeCl_2 \cdot 4H_2O$, 99.5%), ferric nitrate nonahydrate ($Fe(NO_3)_3 . 4H_2O$, 99.9%), cerium chloride ($CeCl_3 \cdot 7H_2O$99.5%) and polyvinylidene fluoride (PVDF, $(CH_2CF_2)_n$) were purchased from Sigma Aldrich. All materials were used as received, without any purification.

2.2. Electrosynthesis of Ce-IO sample

The previously reported cathodic deposition route [63-65], was here modified and developed for the electro-synthesis of cerium doped iron oxide. The synthesis set-up was composed of a (316 L, 5 cm×5 cm×0.5 mm) steel cathode centered between two parallel graphite anodes. The electrolyte bath was prepared by mixing 2 g iron(III) nitrate+1 g iron(II) chloride +0.3 g cerium chloride in 1 liter water as solvent solution. The electro-synthesis process was conducted on an electrochemical workstation system (Potentiostat/Galvanostat, Model: NCF-PGS 2012, Iran) with applying *dc* current density of 10 mA cm^{-2}. The synthesis time and bath temperature were 30 min and 25 ^oC, respectively. After each synthesis, the steel electrode was bring out from the electrolyte and rinsed several times with deionized H_2O. Then, the deposited black film was scraped form the steel and subjected to separation and purification steps, which include; (a) the obtained wet powder was dispersed in deionized water and centrifuged at 6000 rpm for 20 min to removal of free anions, (b) the deposit was then separated from water solution by a magnet, dried at 70 ^oC for 1h, and (c) the resulting black dry powder was named Ce-IO, and used for further evaluations.

2.3. Characterization analyses

The SEM images of the prepared powder were provided through field-emission scanning electron microscopy (FE-SEM, Mira 3-XMU with accelerating voltage of 100 kV). The crystal structure of the prepared Ce-IO powder was determined by X-ray diffraction (XRD, Phillips PW-1800) using a Co Kα radiation. The magnetic properties of the prepared Ce-IO was assessed in the range of −20000 to 20000 Oe at room temperature using vibrational sample magnetometer (VSM, Meghnatis Daghigh Kavir Co., Iran).

2.4. Electrochemical tests

Cyclic voltammetry (CV), galvanostatic charging/discharging (GCD) and electrochemical impedance spectroscopy (EIS) were used for electrochemical characterization of the prepared samples. These tests were done using an electrochemical station (AUTOLAB®, Eco Chemie,

PGSTAT 30) in a three-electrode set up containing a Na_2SO_3 (1 M) aqueous electrolyte. The three-electrode set-up was composed of working electrode (Cerium doped Fe_3O_4 nanoparticles paste electrode), Ag/AgCl reference electrode (saturated with 1 M KCl), and a counter electrode (platinum wire). The working electrode (WE) was fabricated through the well-known paste procedure [34,37]; First, the prepared black Ce-IO powder was physically mixed with acetylene black (>99.9%) and conducting graphite (with rations of 75:10:10), and the mixture was homogenized properly. Then, 5 wt.% polyvinylidene fluoride (PVDF) dissolved inN-Methyl-2-pyrrolidone (NMP)was added into the mixture. After partially evaporating the NMP content of the mixture, the resulting paste was pressed at 10 MPa onto Ni foam (surface area of 1 cm^2). The resulting electrode was dried for 5 min at about 150 °C in oven. In final, the fabricated electrode was used as working electrode in the electrochemical tests. The mass loading of Ce-IO powder onto the Ni foam was about 2.1 mg. The CVs of the fabricated working electrode were recorded in a 1 M Na_2SO_3 electrolyte in the potential range of -1.0 to +0.1 V *vs*. Ag/AgCl. The CV profiles were recorded at the potential sweeps of 2, 5, 10, 20, 50 and 100 mV s^{-1}. The GCD curves were recorded at the different current loads of 0.5, 1, 2, 3 and 5 A g^{-1} within a potential range of -1.0 to 0 V *vs*. Ag/AgCl. The EIS was conducted in the frequency range between 100 KHz and 0.01 Hz with applying 5 mV at open-circuit potential.

3. RESULTS AND DISCUSSION

3.1. Structural and morphological characterizations

Fig. 1 shows the XRD pattern of electro-deposited Ce-IO sample. All the observed diffraction peaks in the XRD pattern could be readily referred to the pure cubic phase [space group: Fd3m (227)] of Fe_3O_4 with cell constants *a*=8.389 Å (JCPDS 01-074-1910). The average crystallite size (D) of the Ce-IO was calculated using the Debye–Scherrer equation, $D=0.9\lambda/\beta\cos(\theta)$, where λ is the X-ray wavelength, β is the full width at half maximum of the diffraction line, and θ is the diffraction angle of the XRD pattern. From the diffraction line-width of (311) peak, the average crystallite size of the prepared Ce-IO was calculated to be 12.2 nm.

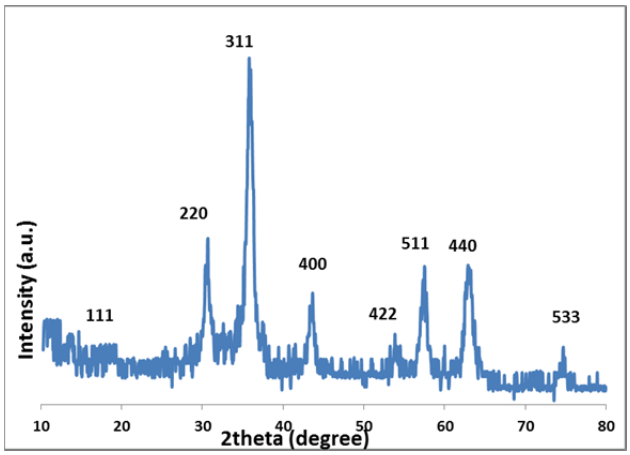

Fig. 1. XRD pattern of the electro-synthesized cerium doped iron oxide

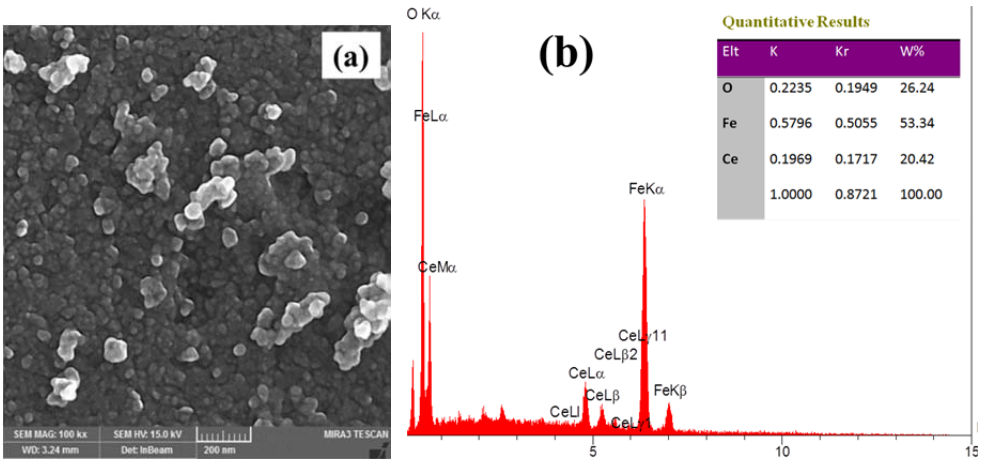

Fig. 2. (a)FE-SEM image and (b) EDS analysis of the prepared cerium doped sample

Fig. 2a presents FE-SEM image of the electrosynthesized sample. It is seen that the electrodeposited sample have particle morphology and the particle size in the range of 20-30nm. The elemental analysis of the prepared nanoparticles was provided through energy-dispersive X-ray (EDX), which is presented in Fig. 3b. In this data, it is seen that the electro-deposited Ce-IO has the Fe, Ce and O atoms with the weight percentages of 53.34%w, 20.42%w and 26.24%w, respectively. These data clearly proved the formation of iron oxide doped with ~20% cerium.

The magnetic hysteresis loop for the prepared Ce-IO sample is shown in Fig. 3. No hysteresis is seen in the VSM profile and the curves have S like form, as seen in Fig. 3. These observations implicated that the prepared Ce-IO has superparamagnetic behavior. The magnetic data of the prepared Ce-IO sample are listed in Table 1. Notably, the magnetic data of bare IO has been provided from Refs [65,66].

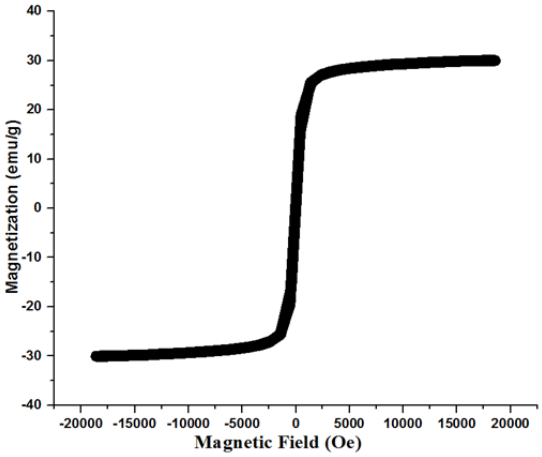

Fig. 3. VSM curve for the prepared cerium doped iron oxide

Table 1. Magnetic data of pure and cerium doped iron oxide[a]

Sample name	**Ms(emu/)g**	**Coercivity (Hci)G**	**Positive (Hci) G**	**Negative (Hci)** G	**Negative Mr(emu/g)**	**Positive Mr(emu/g)**	**Retentivity Mr(emu/g)**
Bare IOs	72.96	14.6	-41.87	-12.66	0.83	2.73	0.95
Ce-IOs	30.03	2.44	10.01	-13.32	0.532	0.49	0.14

[a] The magnetic data of pure iron oxide has been provided from Refs. [65,66]

For the Ce-IO sample, the magnetic data i.e. saturation magnetization (*Ms*), remanent magnetization (*Mr*) and coercivity (H_{Ci}) are recorded to be; *Ms*=30.3 emu g^{-1}, *Mr*=0.14 emu g^{-1} and H_{Ci}=2.44 G. These data confirmed the superparamagnetic nature of the electrodeposited Ce-IO sample. Also, our Ce-IO sample exhibit better superparamagnetic characteristics i.e. higher *Ms* and lower *Mr* and *Hci* values as compared the related data reported in the literature i.e. Sm^{3+} doped IOs (Ms=31.3 emu g^{-1} and Hci=85.7 G) [69], Eu^{3+} doped IOs(Ms=23.6 emu g^{-1} and Hci=74.3 G) [70], Gd^{3+} doped IOs (Ms= 32.9 and 28.9 emu g^{-1} at 100 and 300 K) [71], Cu^{2+} doped IOs (Ms=53.2 emu g^{-1}) [72], and Mn^{2+} doped IOs (Ms=61.5 emu g^{-1}) [72]. Furthermore, these magnetic data are comparable with those of pure IOs electro-synthesized at a similar electrochemical condition in reported previous works. The hysteresis behavior of pure IOs have been previously studied by Aghazadeh et al. [65,66], and the reported data are *Ms*=72.96 emu g^{-1}, *Mr*=0.95 emu g^{-1} and H_{Ci}=14.6 G. The Ce-IO sample exhibited low *Ms* compared with undoped IOs, which can be referred to the Ce atoms low magnetism compared with Fe ones. However, Ce-IO sample show smaller *Mr* and *Hci* values as compared with the pure IOs, which implicated their better superparamagnetic nature.

3.2. Electrochemical evaluation

3.2.1. Cyclic voltammetry

Cyclic voltammetry was used to evaluate the supercapacitive performance of the working electrode (WE) fabricated from the electrosynthesized Ce-IO sample. Fig. 4a presents the CV profiles of the prepared working electrode within the potential range of -1.0 to +0.1 V *vs.* Ag/AgCl with applying the scan rates of 2-100 mV s^{-1}. The shapes of the CV curves clearly reveal the pseudocapacitive properties of the Ce-MNPs, which is different from the electric double-layer capacitance. In the literature, a combination of both EDLC and pseudocapacitance involving the reduction/oxidation of specifically adsorbed SO_3^{2-} anions on the iron oxide surface has been reported for the capacitance behavior of pure magnetite electrode in the Na_2SO_3 solution [39-41], which are seen by small peaks on the CV curve.

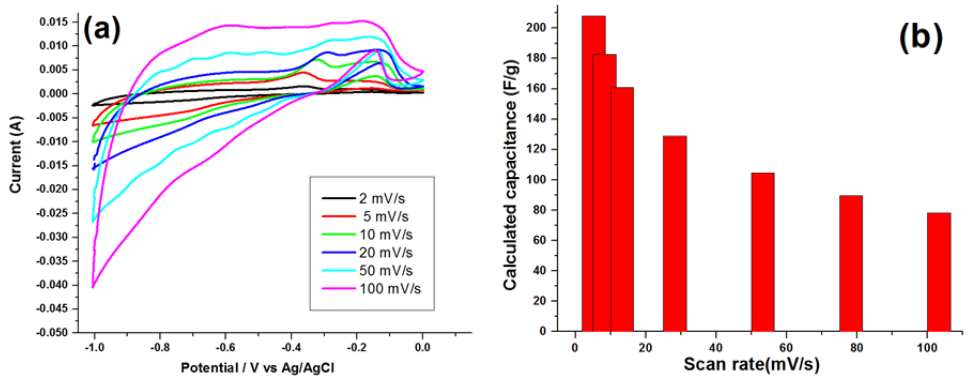

Fig. 4. (a) CVs of Ce-IO electrode at the various scan rates and (b) the calculated specific capacitances

For Ce-IO electrode, there are some small peaks on cyclic voltammograms, which due to the following reactions [37,65,66]:

$$2SO_3^{2-}+3H_2O+4e^- \leftrightarrow S_2O_3^{2-} + 6OH^- \quad (1)$$

$$S_2O_3^{2-} + 3H_2O + 8e^- \leftrightarrow 2S^- + 6OH^- \quad (2)$$

The SC values were calculated from their CV profiles by Eq. (3) [24]:

$$C = \frac{Q}{m\Delta\,(V)}, \quad Q = \int_{V_a}^{V_a} I(V)dV \quad (3)$$

Where C is the capacitance of prepared Ce-IO powder (F g^{-1}), Q is the total charge, ΔV is the potential window, *m* is the mass of Ce-IO powder (g), v is the scan rate (V s^{-1}) and I(V) is the current response during the potential scan. Then, the SCs were plotted *vs.* scan rate, as shown in Fig. 4b. The calculations revealed that the Ce-IO electrode are capable to give SC values as high as 208, 182, 161, 132, 104, 89 and 78 F g^{-1} at the scan rates of 2, 5, 10, 20, 50,

75 and 100 mV s^{-1}, respectively. Notably, it was reported that the undoped IO electrode is enable to deliver SC values of 181, 159, 140, 112, 92, 83 and 68 F g^{-1} at the scan rates of 2, 5, 10, 20, 50 and 100 mV s^{-1}, respectively [65,66]. Comparing these SC values revealed that the Ce-IO electrode provide up to 15% larger SC values as compared with those of undoped IO electrode.

3.2.2. Charge-discharge tests

Galvanostatic charge-discharge (GCD) profiles of Ce-IO electrode were recorded at current loads of 0.5, 1, 2, 3, 5 and 10 A g^{-1} and are given in Fig. 5a.

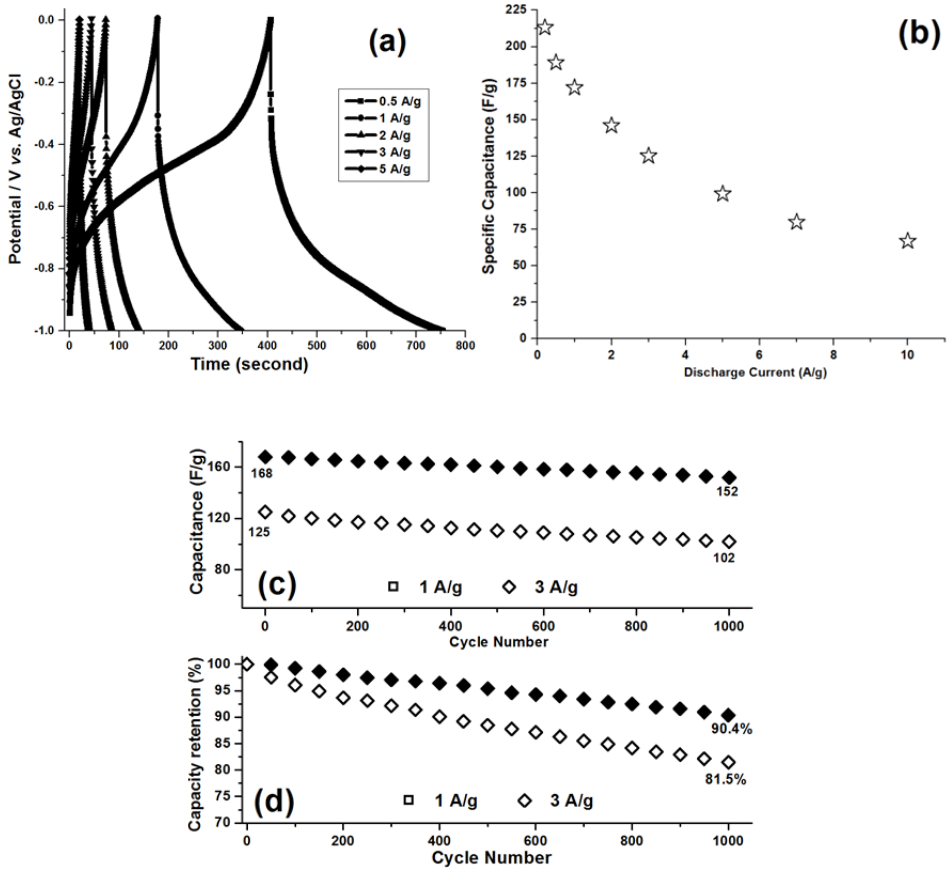

Fig. 5. (a) GCD profiles of Ce-IO electrode and (b) its calculated SCs at the different current loads of 0.5 to 5 A g^{-1}; (c) capacity values and (d) capacity retention for 1000 GCD cycling at 1 and 3 A g^{-1}

These GCD profiles can be divided into two parts; first a symmetric triangular form at region of V<-0.4 V *vs*. Ag/AgCl, and second, nonlinear dependency of potential at region of V≥-0.4 V *vs*. Ag/AgCl, which are similar to the previously reported GCD profiles for Sm, Mn, Ni and Co doped IO electrodes [65-68]. The first section indicates the pure EDLC

behavior and the second part shows the pseudocapacitance performance (Eqs. 1 and 2). The SCs were calculated using Eq. (4) [33], and the data is presented in Fig. 5b:

$$C = \frac{Q}{m \times \Delta V}, Q = I \times \Delta t \quad (4)$$

Where C is the capacitance of prepared Ce-IO powder (F g^{-1}), Q is the total charge, ΔV is the potential window, *m* is the mass of Ce-IO powder (g), v is the scan rate (V s^{-1}) and I is the applied current load (A) and Δt is the time of a discharge cycle. The calculations revealed that the Ce-IO electrode are capable of delivering SC values of 216 F g^{-1}, 191 F g^{-1}, 168 F g^{-1}, 146 F g^{-1}, 125 F g^{-1}, 99 F g^{-1}, 79 F $g^{-1}$and 67 F g^{-1} at the discharge loads of 0.2, 0.5, 1, 2, 3, 5, 7 and 10 A g^{-1}, respectively. These values showed the proper SC behavior for the electro-synthesized Ce-IO sample.

The fabricated working electrode was further cycled (1000 cycles) at the current loads of 1 and 3 A g^{-1} in 1M Na_2SO_3 electrolyte. The SC values and capacity retentions of the fabricated Ce-IO electrode calculated during cycling. Figs. 5c and d represent the SCs and SC retentions *vs*. cycle number, respectively. It was found that the SC value of Ce-IO electrode is reduced from 168 F g^{-1} to 152 F g^{-1} after 1000 GCD cycling at a discharging current of 1 A g^{-1} (Fig. 5c), which exhibited about 90.4% capacity retention, as seen in Fig. 5d. Also, the fabricated Ce-IO electrode is enable to deliver specific capacitance as high as 102 F g^{-1} after 1000 GCD cycles at a current load of 3 A g^{-1}, which showed that the electrode had capacity retention of 81.5% at this discharging current (Fig. 5d). These data confirmed the proper charge storage ability of Ce-IO electrode.

3.2.3. EIS measurement

Fig. 6 shows the typical Nyquist plot of the Ce-IO electrode in the 1 M Na_2SO_3 electrolyte within the frequency range of 1Hz −100KHz. This plot has two parts of a semicircle in the high frequency region and a straight line in the low frequency region. An equivalent circuit including electrolyte resistance (R_s), double layer capacitor (C_{dl}), charge transfer resistance (R_{ct}), Warburg element (Z_w) and a pseudocapacitor (C_p) could be used for fitting of this Nyquist plot, which is shown in the inset of Fig. 6. The low diffusion resistance of Ce-IO electrode is elucidated from the nearly straight line at the lower frequency zone. The enlarged part of semicircle in the high frequency region provides the values of 2.97 Ω and 3.5 Ω for ESR and R_{ct} respectively. These low resistances are indicative of the fast redox reaction, charge storage and proper charge storage ability for the prepared Ce-IO electrode.

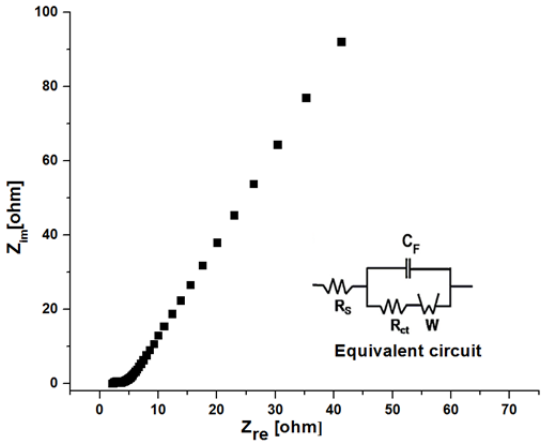

Fig. 6. Nyquist plot of the Ce-IO electrode

4. CONCLUSION

In summary, a novel electrosynthesis procedure was reported for the preparation of cerium doped iron oxide. The XRD, FE-SEM and EDS analyses proved the magnetite phase, fine particle morphology (i.e. 20 nm in size) and cerium cations (20%wt) doping in its structure. Galvanostat charge-discharging the fabricated electrode indicated that the Ce-IO electrode is capable are capable to give SC values as high as 216, 191, 168, 146, 125, 99, 79 and 67 F g^{-1} at the discharge loads of 0.2, 0.5, 1, 2, 3, 5, 7 and 10 A g^{-1}, respectively. It was found that the charge storage and magnetic abilities of iron oxide are improved by metal cations doping.

REFERENCES

[1] S. Zheng, Z. S. Wu, S. Wang, H. Xiao, F. Zhou, C. Sun, X. Bao, and H. M. Cheng, Energy Storage Mater. 6 (2017) 70.

[2] P. J. Sephra, P. Baraneedharan, M. Sivakumar, T. D. Thangadurai, and K. Nehru, Mater. Res. Bull. 106 (2018) 103.

[3] Z. Shi, L. Xing, Y. Liu, Y. Gao, and J. Liu, Carbon 129 (2018) 819.

[4] M. Aghazadeh, R. Ahmadi, D. Gharailou, M. R. Ganjali, and P. Norouzi, J. Mater. Sci.: Mater. Electron. 27 (2016) 8623.

[5] M. Aghazadeh, M. Hosseinifard, B. Sabour, and S. Dalvand, Appl. Surf. Sci. 287 (2013) 187.

[6] K. Prasanna, P. Santhoshkumar, Y. Nam Jo, I. N. Sivagami, and C. W. Lee, Appl. Surf. Sci. 449 (2018) 454.

[7] M. Aghazadeh, and M. R. Ganjali, J. Mater. Sci.: Mater. Electron. 28 (2017) 8144.

[8] J. Lv, Z. Wang, and H. Miura, Solid State Commun. 269 (2018) 45.

[9] M. Aghazadeh, J. Mater. Sci.: Mater. Electron. 28 (2016) 3108.

[10] P. Prasannalakshmi, N. Shanmugam, and N. Kannadasan, J. Electroanal. Chem. 775 (2016) 356.
[11] J. Liang, Y. Chai, D. Li, M. Li, J. Lu, L. Li, and M. Luo, Appl. Surf. Sci. 414 (2017) 68.
[12] M. Aghazadeh, A. Bahrami-Samani, D. Gharailou, M. G. Maragheh, and M. R. Ganjali, J. Mater. Sci.: Mater. Electron. 27 (2016) 11192.
[13] R. Poonguzhali, N. Shanmugam, R. Gobi, A. Senthilkumar, G. Viruthagiri, and N. Kannadasan, J. Power Sources. 293 (2015) 790.
[14] M. Aghazadeh, M. R. Ganjali, and P. Norouzi, J. Mater. Sci.:Mater. Electron. 27 (2016) 7707.
[15] M. Aghazadeh, M. G. Maragheh, M. R. Ganjali, P. Norouzi, and F. Faridbod, Appl. Surf. Sci. 364 (2016) 141.
[16] H.R. Naderi, P. Norouzi, and M.R. Ganjali, Appl. Surf. Sci. 366 (2016) 552.
[17] R. Poonguzhali, R. Gobi, N. Shanmugam, A. Senthil Kumar, G. Viruthagiri, and N. Kannadasan, Mater. Lett. 157 (2015) 116.
[18] M. Aghazadeh, I. Karimzadeh, A. Ahmadi, M. R. Ganjali, P. Norouzi, J. Mater. Sci.: Mater. Electron. 29 (2018) 14378.
[19] M. Aghazadeh, I. Karimzadeh, A. Ahmadi, and M. R. Ganjali, J. Mater. Sci.: Mater. Electron. 29 (2018) 14567.
[20] T. Nguyen, M. Boudard, M. J. Carmezim, and M. F. Montemor, Scientific Reports. (2017) doi:10.1038/srep39980
[21] M. Aghazadeh, A. Nozad, H. Adelkhani, and M. Ghaemi, J. Electrochem. Soc. 157 (2010) D519.
[22] M. Aghazadeh, A. A. M. Barmi, and M. Hosseinifard, Mater. Lett. 73 (2012) 28.
[23] M. Aghazadeh, and S. Dalvand, J. Electrochem. Soc. 161 (2014) D18.
[24] M. Aghazadeh, S. Dalvand, and M. Hosseinifard, Ceram. Int. 40 (2014) 3485.
[25] M. Aghazadeh, H. Mohammad Shiri, and A. A. Malek Barmi, Appl. Surf. Sci. 273 (2013) 237.
[26] T. Yin, W. Zhang, Y. Yin, Y. Yan, K. Zhan, J. Yang, and B. Zhao, J. Mater. Sci.: Mater. Electron. 28 (2017) 7884.
[27] J. T. Mehrabad, M. Aghazadeh, M. G. Maragheh, and M. R. Ganjali, Mater. Lett. 184 (2016) 223.
[28] L. Gong, and L. Su, Appl. Surf. Sci. 257 (2011) 10201.
[29] M. Aghazadeh, A. Nozad Golikand, and M. Ghaemi, Int. J. Hydrogen Energy 36 (2011) 8674.
[30] J. Tizfahm, B. Safibonab, M. Aghazadeh, A. Majdabadi, B. Sabour, and S. Dalvand, Colloids and Surf. A 443 (2014) 544.
[31] M. Aghazadeh, M. Asadi, M. R. Ganjali, P. Norouzi, B. Sabour, and M. Emamalizadeh, Thin Solid Films 634 (2017) 24.

[32] M. Aghazadeh, M. Ghaemi, B. Sabour, and S. Dalvand, J. Solid State Electrochem. 18 (2014) 1569.
[33] M. Aghazadeh, B. Sabour, M. R. Ganjali, and S. Dalvand, Appl. Surf. Sci. 313 (2014) 581.
[34] M. Aghazadeh, I. Karimzadeh, and M. R. Ganjali, J. Mater. Sci.: Mater. Electron. 28 (2017) 13532.
[35] J. Sun, P. Zan, X. Yang, L. Ye, and L. Zhao, Electrochim. Acta 215 (2016) 483.
[36] L. Wang, X. Zhang, S. Wang, Y. Li, and G. Yang, Powder Technol. 256 (2014) 499.
[37] L. Wang, H. Ji, S. Wang, L. Kong, X. Jiang, and G. Yang, Nanoscale 5 (2013) 3793.
[38] J. Chen, K. Huang, and S. Liu, Electrochim. Acta 55 (2009) 1.
[39] X. Zeng, B. Yang, X. Li, R. Li, and R. Yu, Mater. Design 101 (2016) 35.
[40] J. Ma, J. Chang, H. Ma, D. Zhang, Q. Ma, and S. Wang, J. Colloid Interface Sci. 498 (2017) 282.
[41] V. D. Nithya, and N. S. Arul, J. Mater. Chem. A. 4 (2016) 10767.
[42] Y. Yang, J. Li, D. Chen, and J. Zhao, ACS Appl. Mater. Interfaces 8 (2016) 26730.
[43] Y. Z. Wu, M. Chen, X. H. Yan, J. Ren, Y. Dai, J. J. Wang, J. M. Pan, Y. P. Wang, and X. N. Cheng, Mater. Lett. 198 (2017) 114.
[44] D. Guan, Z. Gao, W. Yang, J. Wang, and L. Liu, Mater. Sci. Eng. B 178 (2013) 736.
[45] I. Oh, M. Kim, and J. Kim, Appl. Surf. Sci. 328 (2015) 222.
[46] M. M. Mezgebe, Z. Yan, G. Wei, S. Gong, and H. Xu, Mater. Today Energy 5 (2017) 164.
[47] X. Lv, G. Li, H. Zhou, D. Li, and Q. Wei, J. Electroanal. Chem. 810 (2018) 18.
[48] M. Aghazadeh, I. Karimzadeh, M. Ghannadi Maragheh, and M. R. Ganjali, Mater. Res. 21 (2018) e20180094.
[49] X. Tang, R. Jia, T. Zhai, and H. Xia, ACS Appl. Mater. Interfaces 7 (2015) 27518.
[50] T. Xia, X. Xu, J. Wang, C. Xu, F. Meng, Z. Shi, J. Lian, and J. M. Bassat, Electrochim. Acta 160 (2015) 114.
[51] W. M. Zhang, X. L. Wu, J. S. Hu, Y. G. Guo, and L. J. Wan, Adv. Funct. Mater. 18 (2008) 3941.
[52] Q. Maqbool, C. Singh, A. Paul, and A. Srivastava, J. Mater. Chem. C 3 (2015) 1610.
[53] H. R. Naderi, A. Sobhani-Nasab, M. Rahimi-Nasrabadi, M.R. Ganjali, Appl. Surf. Sci. 423 (2017) 1025.
[54] P. M. Hallam, M. Gómez-Mingot, D. K. Kampouris, and C. E. Banks, RSC Adv. 2 (2012) 6672.
[55] S. Y. Wang, K. C. Ho, S. L. Kuo, and N. L. Wu, J. Electrochem. Soc. 153 (2006) A75.
[56] S. Liu, S. Guo, S. Sun, and X. Z. You, Nanoscale 7 (2015) 4890.
[57] M. Aghazadeh, and M. R. Ganjali, J. Mater. Sci.: Mater. Electron. 29 (2018) 2291.
[58] M. Aghazadeh, T. Yousefi, and M. Ghaemi, J. Rare Earths 30 (2012) 236.

[59] M. Aghazadeh, M. G. Maragheh, M. R. Ganjali, and P. Norouzi, Inorg. Nano-Metal Chem. 27 (2017) 1085.
[60] M. Aghazadeh, I. Karimzadeh, and M. R. Ganjali, J. Electron. Mater. 47 (2018) 3026.
[61] M. Aghazadeh, Mater. Lett. 211 (2018) 225.
[62] I. Karimzadeh, H. Rezagholipour Dizaji, and M. Aghazadeh, Mater. Res. Express 3 (2016) 095022.
[63] I. Karimzadeh, H. R. Dizaji, and M. Aghazadeh, J. Magn. Magn. Mater. 416 (2016) 81.
[64] M. Aghazadeh, I. Karimzadeh, and M. R. Ganjali, Mater. Lett. 228 (2018) 137.
[65] M. Aghazadeh, and M. R. Ganjali, Ceram. Int. 44 (2018) 520.
[66] M. Aghazadeh, and M. R. Ganjali, J. Mater. Sci. 53 (2018) 295.
[67] M. Aghazadeh, and M. R. Ganjali, J. Mater. Sci.: Mater. Electron. 29 (2018) 4981.
[68] M. Aghazadeh, I. Karimzadeh, M. R. Ganjali, and A. Behzad, J. Mater. Sci.: Mater. Electron. 28 (2018) 18121.
[69] C. R. De Silva, S. Smith, I. Shim, J. Pyun, T. Gutu, J. Jiao, and Z. Zheng, J. Am. Chem. Soc. 131 (2009) 6336.
[70] J. C. Parka, S. Yeo, M. Kim, G. T. Lee, and J. H. Seo, Mater. Lett. 181 (2016) 272.
[71] F. J. Douglas, D. A. MacLaren, N. Maclean, I. Andreu, F. J. Kettles, F. Tun, C. C. Berry, M. Castro, and M. Murrie, RSC Adv. 6 (2016) 74500.
[72] T. M. Thi, N. T. Huyen Trang, and N. T. Van Anh, Appl. Surf. Sci. 340 (2015) 166.